JOURNAL OF MASS SPECTROMETRY
*J. Mass Spectrom.* **33**, 921–935 (1998)

# Study of Ghost Peaks Resulting from Space Charge and Non-linear Fields in an Ion Trap Mass Spectrometer

**F. Kocher, A. Favre, F. Gonnet and J.-C. Tabet***
Laboratoire de Chimie Structurale Organique et Biologique, UMR 7613 (CNRS), Université Pierre et Marie Curie, 4 Place Jussieu, 75252 Paris Cedex 05, France

**Ion trap improvements require some geometrical modifications which can alter significantly the relative linear and non-linear field contributions. In this work, where the ion trap was interfaced with an electrospray source, it was shown that under particular ion trapping conditions due to space charge, artefacts called ghost peaks are displayed in the mass spectra. They are characterized by particular width and shape and appear at twice the $m/z$ ratio of the expected peaks (for positive and negative ions) when the analyzed ions are ejected at $\beta_z = 1/3$ (extended mass range mode). They were unambiguously identified by using isolation sequences. The various experimental factors governing the observation of ghost peaks were explored in order to rationalize their origin. Especially the capillary exit voltage, ion accumulation time and low $m/z$ cut-off of the analytical scan, which modify the space charge strength, influence the ghost peak intensities. Furthermore, it is evidenced that only the injected ions which are located at $q_z \leqslant 0.25$ ($\beta_z \leqslant 2/11$) at the beginning of the analytical scan step give rise to the formation of such artefact peaks. Under these experimental conditions, the ion cloud defocused by space charge is subjected to high-order multipole fields (e.g. 22-pole). Then the motion of the analyzed ions is destabilized, affecting the ion ejection. It seems that two ion populations can co-exist: (i) one submitted to a normal ion ejection at $q_z = 0.45$, where the axial modulation is applied, i.e. normal peaks, and (ii) a second ejected at the natural $q_z = 0.908$ boundary, leading to ghost peaks at twice the $m/z$ value of normal signals.** © **1998 John Wiley & Sons, Ltd.**

KEYWORDS: ion trap; non-linear fields; space charge; extended mass range; electrospray ionization

## INTRODUCTION

The interest in the use of the ion trap mass spectrometer for analyzing ions characterized by high $m/z$ ratios, in both positive and negative ion modes (i.e. cationized or protonated and deprotonated molecules, respectively) has been growing rapidly. Especially with this kind of analyzer, quasi-molecular species can be externally produced from non-volatile and labile compounds such as biomolecules (e.g. peptides,[1] proteins[2] and oligonucleotides[3]) submitted to desorption/ionization techniques [i.e. electrospray ionization (ESI)[4] and matrix-assisted laser desorption/ionization (MALDI)[5]]. Using ESI, molecules are desorbed as multiply charged ions and detected at the corresponding $m/z$ values. This desorption technique should allow mass spectrometric (MS) analysis of large biomolecules (with molecular masses $>10^6$ u).[6] Electrospray sources are usually coupled with quadrupole analyzers, whose detection limit is about 2000–4000 Th. Commercial ion traps combined with external ESI sources are now available. A consequence of the intrinsic properties of quadrupole ion traps is their limited $m/z$ range, according to the following relationship:

$$[m/z]_{max} = 8\ eV_{max}/[q_{z,\,eject}(R_0^2 + 2Z_0^2)\Omega^2] \quad (1)$$

where $\Omega$ is the angular frequency of the r.f. voltage (V), $2Z_0$ is the distance between the end-caps, $R_0$ is the internal ring electrode radius and $[m/z]_{max}$ is the maximum $m/z$ ratio reached at the $V_{max}$ value (zero-to-peak) of the r.f. drive potential. This working point, without application of a d.c. voltage (i.e $U = 0$), corresponds to the $q_{z,\,eject}$ trapping parameter at which the ion motion becomes unstable according to the Mathieu stability diagram. Mass range extension can be achieved in different ways. Modification of four parameters related to Eqn (1) could extend the mass-to-charge range[7] of the ion trap:

(a) Either by reducing (i) the trap internal size, i.e. both the $R_0$ and $Z_0$ dimensions (e.g. a quarter-sized trap yields a 16-fold increase in $[m/z]_{max}$ close to 10 000 Th)[8a], (ii) the $\Omega$ angular frequency value (e.g. a reduction from 1.1 to 0.6 MHz leads to more than a three-fold increase in the $m/z$ range) and (iii) the $q_{z,\,eject}$ value: for a given $q_{z,\,eject}$ value, a corresponding $[m/z]_{max}$ value can be achieved according to $q_{z,\,eject} = 0.908 \times 650/[m/z]_{max}$.[8] Todd *et al.*[9] introduced the reverse

* *Correspondence to*: J.-C. Tabet, Laboratoire de Chimie Structurale Organique et Biologique, UMR 7613 (CNRS), Université Pierre et Marie Curie, 4 Place Jussieu, 75252 Paris Cedex 05, France
E-mail: tabet@ccr.jussieu.fr
Contract/grant sponsor: Centre d'Etudes du Bouchet.
Contract/grant sponsor: Université Pierre et Marie Curie.
Contract/grant sponsor: CNRS.

CCC 1076–5174/98/100921–15 $17.50


*Received 23 January 1998*
*Accepted 15 June 1998*

scan method, in which a positive d.c. potential is superimposed on the r.f. voltage to the ring electrode. During the analytical scan, both the r.f. and d.c. voltages are decreased by maintaining the $U/V$ ratio constant. This linked scan method allows ion ejection at the $\beta_z = 0$ stability boundary to detect ions of $[m/z]_{max}$ close to 2000 Th.

(b) Or by increasing the r.f. voltage, a solution which has not been used, because high voltage could not be increased above 10 kV with an He buffer gas pressure of $10^{-3}$ Torr (0.13 Pa).

Note that for (iii), the $\beta_z$ values used for the mass-selective instability scan can correspond to non-linear resonances with working points lower than the $q_z = 0.908$ limit. Furthermore, axial modulation, using a dipolar frequency, can be applied to produce fast ejection, improving the $m/z$ ratio resolution (e.g. $\Delta m/z$ better than 0.2 Th) and enhancing the ejection efficiency.[10]

Here, with a 781 kHz trapping r.f. frequency, the non-linear ion trap mass spectrometer used provides three $m/z$ analysis ranges:[11] (i) standard mode up to 2000 Th (resonance ejection at $\beta_{z,\,eject} = 2/3$, corresponding to $q_z = 0.78$, with 260.3 kHz as the dipolar frequency for axial modulation), (ii) extended mode up to 3400 Th (resonance ejection at $\beta_{z,\,eject} = 1/3$, corresponding to $q_z = 0.45$, with 130.1 kHz) and (iii) high mass range up to 6000 Th (resonance ejection at $\beta_{z,\,eject} = 2/11$, corresponding to $q_z = 0.25$, with 71 kHz as axial modulation). The various selected $\beta_{z,\,eject}$ values correspond to non-linear resonances (i.e. considered as black holes[12] or black canyons[13]) caused by higher order multipole fields (e.g. hexapole, dodecapole) due to the end-cap and ring electrode geometries, end-cap perforations and external fields in front of the holes. These particular non-linear resonances can result in efficient ejection of the trapped ions by simple application of a particular axial modulation with $\omega_{z,\,eject}$ related to the chosen $\beta_{z,\,eject}$ values:[7a]

$$\omega_{z,\,eject} = \beta_{z,\,eject}\Omega/2 \qquad (2)$$

For biomolecules yielding peaks at $m/z$ values $<6000$ Th, deconvolution of the multiply charged ion distribution provides molecular weight determination.[14] However, to obtain more structural information, fragmentations of the desorbed molecular species are required. They can take place through CID process either in the skimmer region[15] by increasing the voltage between the transfer capillary exit and the skimmer entrance, or at the center of the ion trap, by subjecting the selected parent ions to resonant[16] (or non-resonant)[17] excitations. In the latter mode, sequential $MS^n$ experiments (with $n \geqslant 2$)[18] efficiently lead to specific structural information.

The present investigations allow the elucidation of the positive and negative ion mass spectra of peptides and oligonucleotides, respectively, recorded within space charge conditions (induced by a high number of injected ions prepared from an external ESI source). The space charge effects due to ion–ion interactions have been widely reported.[12,13,19,20] They can be viewed as moving the stability diagram towards the higher $q_z$ values associated with a 'narrowing' of its surface (i.e. a decrease in the $q_z$ parameter range for trapping ions).[21] The main resulting effects are the following: (i) erroneous $m/z$ measurements which correspond to mass shifts,[22] (ii) distortion of peak shapes[23] and (iii) a loss of the higher $m/z$ ions when the lower $m/z$ ions are abundant.[20]

Ion–ion interactions also lead to large ion excursions away from the center of the ion trap and ions approach the end-caps in addition to the ring electrode. Then the defocused ions are subjected to an unknown distribution of superimposed multipole fields. Consequently, their secular frequencies differ from those at the center of the ion trap, so the mass shift occurs in addition to other phenomena such as appearance of additional peaks as artefacts.

Recently, Mo *et al.*[24] showed that during a conventional analytical r.f. amplitude scan (i.e. $q_{z,\,eject} = 0.908$), when the r.f. voltage is ramping through a $q_z$ value corresponding to a non-linear resonance on the stability diagram, some ions are ejected before reaching the $\beta_z = 1$ boundary. Then, their measured $m/z$ ratio appears to be lower than expected [e.g. with FC-43 under EI conditions, the $CF_3^+$ ($m/z$ 69) ion is partially located at $m/z$ 60–61 because of the hexapole resonance $\beta_z = 2/3$ (i.e. $q_z = 0.78$)]. This is another aspect of the 'black holes' phenomenon which is particularly pronounced at $\beta_z = 2/3$ compared with the other non-linear resonances. Furthermore, particular unexpected signals have already been observed at higher $m/z$ values,[25] unfortunately without further explanation. Here, such signals, termed ghost peaks and observed in ESI mass spectra with a conventional ion trap analyzer, were optimized in order to elucidate their origins. This will also provide information on non-linear field properties.

## EXPERIMENTAL

### Chemicals

The d(TTGG) oligonucleotide was synthesized at the 100 μmol scale, using phosphoramidate chemistry on a solid support (Milligen 8800).[26] Its purity was monitored by capillary electrophoresis and analytical high-performance liquid chromatography (HPLC) by the group of Igolen and Huynh Dinh (Institut Pasteur, Paris, France). Peptides (FFF and RPKPQQFGLM) were purchased from Sigma. Methanol and propan-2-ol (HPLC purity) were purchased from Prolabo and triethylamine (TEA) and acetic acid from Aldrich-Chimie and were used without further purification. High-purity water was obtained from a Milli-Q system (Millipore).

### Electrospray ionization ion trap mass spectrometry

All experiments were performed on an ESQUIRE ion trap (Bruker, Bremen, Germany). The non-linear ion trap worked in the mass-selective instability mode without using a d.c. voltage (i.e. $U = 0$ condition) at the ring electrode. The analyzer operated at the $a_z = 0$ line for each $m/z$ range mode. As mentioned previously, the multicomponent multipole fields were related to the electrode configurations and geometries (stretched end-caps separation, truncation, end-caps holes and

 

modified hyperbolic angle, as for the ESQUIRE ion trap analyzer).[11]

The instrument has a fundamental r.f. frequency of 781 kHz and was used in three modes: standard mode with a $m/z$ ratio up to 2000 Th[27] [its scan used the non-linear resonance at $\beta_z = 2/3$ ($q_z = 0.78$) for selective resonance ejection of ions with an analytical scan rate of $\sim$ 2000 Th/s]; extended mode with a $m/z$ ratio of up to 3400 Th [its scan used the non-linear resonance at $\beta_z = 1/3$ ($q_z = 0.45$) for selective resonance ejection of ions (analytical scan rate 1700 Th/s)]; and high mode with a $m/z$ ratio of up to 6000 Th/s [its scan used the non-linear resonance at $\beta_z = 2/11$ ($q_z = 0.25$) for selective resonance ejection of ions (analytical scan rate 8000 Th/s)]. For these three modes the low $m/z$ cut-off is 50 Th. The ion trap operated at an uncorrected partial He buffer gas pressure of $3.4 \times 10^{-5}$ Torr ($4.5 \times 10^{-3}$ Pa). A differentially pumped interface transferred ions from the electrospray source (Analytica of Brandford, Brandford, CT, USA) to the mass spectrometer. In the MS/MS mode, the isolation step was performed by broadband ejection of ions, with an ion isolation window of 50 Th width.

### Infused solutions

Peptides were analyzed in the positive ion mode. Dilute samples ($2.5 \times 10^{-5}$ M) in methanol–water–acetic acid (50:50:1, v/v/v) were infused into the ESI source using a Cole-Parmer 74900 Series syringe pump at a flow-rate of 50 µl $h^{-1}$. The capillary entry voltage was about $-3500$ V. The $N_2$ drying gas temperature was 200 °C with a flow-rate of 200 l $h^{-1}$.

The d(TTGG) oligonucleotide was analyzed in the negative ion mode. Dilute samples ($5 \times 10^{-5}$ M) in propan-2-ol–water–triethylamine (50:50:1, v/v/v) were infused into the ESI source at a flow-rate of 100 $\mu$l $h^{-1}$. The capillary entry voltage was about 2200 V. The $N_2$ drying gas temperature was 200 °C with a flow-rate of 500 l $h^{-1}$ and the nebulizing gas had a working pressure of 20 psi ($1.38 \times 10^5$ Pa).

Some applied parameters were unchanged in both modes, such as the r.f. frequency amplitude of the hexapole (350 V) and the voltage applied on the electron multiplier ($-1500$ V). In the positive ion mode the d.c. voltage applied to the ion guide (hexapole) was 2 V, the dynode voltage of the electron multiplier was $-5$ kV, the delay before scanning was 10 ms and the exit lens voltage was $-200$ V. In the negative ion mode, these values were $-2$ V, 5 kV, 100 ms and 150 V, respectively.

## RESULTS AND DISCUSSION

The aim of this study was to investigate the role played by non-linear resonances in the positive and negative ion ESI mass spectra of peptides and oligonucleotides, respectively. Modifications of various experimental parameters were studied. They strongly affect the sensitivity and reproducibility of ESI mass spectra, especially when the ion trap is operated under large space charge conditions. Furthermore, such experimental conditions lead to unexpected phenomena (e.g. mass spectrum distorsion and the occurrence of 'ghost peaks'), accompanying the analysis of the injected ions prepared in the ESI external source.

It is helpful to examine ESI mass spectra recorded in the conventional mode (i.e. standard mode) with positive and negative ions, in order to describe the desorbed quasi-molecular species, in addition to the fragment ions generated from the ESI external source and in the skimmer desolvation zone, respectively.[15] The ESI mass spectra of positive ions of substance P ($M_r = 1348$ u) and negative ions of d(TTGG) ($M_r = 1204$ u) are reported in Fig. 1(a) and 1(b), respectively. Ions were externally prepared, injected and trapped in the ion trap mass spectrometer (without using an ion gain control device)[28] and then analyzed by an analytical r.f. level scan with ion ejection at $\beta_z = 2/3$ (i.e. standard mode). The mass spectrum of substance P, recorded without abundant space charge [Fig. 1(a)], mainly displays four peaks at $m/z$ 447, 451, 601 and 676 corresponding to the triply charged $[M + 3H - H_2O/NH_3]^{3+}$ fragment ion (exact assignment uncertain), the triply charged $[M + 3H]^{3+}$ molecular species, the $\mathbf{b}_{10}^{2+}$ fragment ion (Roepstorff notation)[29] and the doubly charged $[M + 2H]^{2+}$ molecular species, respectively.[30] The peaks detected at lower $m/z$ range are impurities.

The negative ion ESI mass spectrum of d(TTGG) [Fig. 1(b)] displays three peaks at $m/z$ 404, 602 and 614 corresponding to the triply charged $[M - 3H]^{3-}$ and the doubly charged $[M - 2H]^{2-}$ and $[M + Na - 3H]^{2-}$ ions, respectively. They are observed without fragmentation, showing their own stability towards collision occurring in the injection step in the ion trap.

The recorded mass spectra are, as expected, very dependent on the ESI source conditions (e.g. capillary exit voltage and skimmer potential), the ion trap injection conditions (e.g. ion accumulation time, injection r.f. level and $m/z$ range) and the ion ejection conditions such as the low $m/z$ value of the analytical scan. Furthermore, when ions are analyzed using the extended mode (i.e. $\beta_{z,\,\mathrm{eject}} = 1/3$ and $q_{z,\,\mathrm{eject}} = 0.45$), additional signals sometimes appeared, although the ion preparation and injection conditions were identical with those in the standard mode (i.e. $\beta_{z,\,\mathrm{eject}} = 2/3$, and $q_{z,\,\mathrm{eject}} = 0.78$). Such signals considered here as artefacts, called 'ghost peaks',[24] are characterized by properties (i.e. intensity, resolution and exact $m/z$ location) related to the experimental conditions.

### Influence of the ion accumulation time on space charge and appearance of artefact peaks

Injection of the externally prepared ions with the extended mode, which corresponds to ejection at a lower $q_z$ value than that in the standard mode, leads to significant mass spectrum modifications under space charge conditions, such as (i) shift of signal position [Fig. 2(c) and (d)], (ii) decrease in signal resolution [Fig. 2(c) and (d)] and (iii) ion loss [Fig. 2(d)]. These effects can be explained by considering that the space charge is enlarged in this mode, implying a decrease in the stability diagram surface.[12,13,19,20] This assumption is based

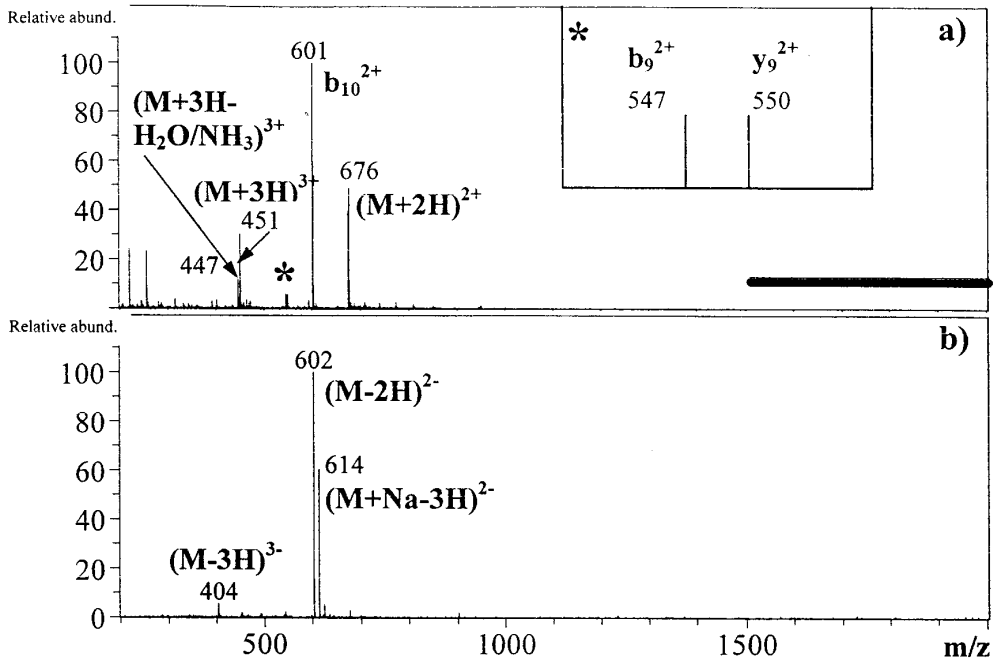


**Figure 1.** ESI mass spectra (average of 10 mass spectra summations) of (a) positive ions of substance P recorded in standard mode ($\beta_{z,\,\mathrm{eject}} = 2/3$) within the 100–1500 Th range, at a capillary exit voltage of 60 V, a skimmer voltage of 10 V, an accumulation time of 10 ms and a low $m/z$ cut-off value of 50 Th; and (b) negative ions of d(TTGG) recorded in standard mode ($\beta_{z,\,\mathrm{eject}} = 2/3$) within the 200–2000 Th range, at a capillary exit voltage of −100 V, a skimmer voltage of −10 V, an accumulation time of 100 ms and a low $m/z$ cut-off value of 50 Th.

upon variation of the trapping $q_{z,\,\mathrm{injec}}$ parameter which influences the depth of the pseudo-potential well ($\bar{D}_{z,\,\mathrm{injec}}$),[31] particularly when $a_z = 0$ and $q_z \leqslant 0.4$ (i.e when satisfying the adiabatic approximation $\beta^2_{z,\,\mathrm{injec}} = q^2_{z,\,\mathrm{injec}}/2$). When trapping only one ion species at the $m_a/z_a$ position, the depth of the pseudo-potential well is

$$|\bar{D}_{z,\,\mathrm{injec}}| = \frac{m_a \Omega^2 q^2_{z,\,\mathrm{injec}} {Z_0}^2}{16 z_a e} \tag{3a}$$

$$|\bar{D}_{r,\,\mathrm{injec}}| = \frac{m_a \Omega^2 q^2_{r,\,\mathrm{injec}} {R_0}^2}{16 z_a e} \tag{3b}$$

As the magnitude of $q_z$ is twice that of $q_r$ (in absolute value), the depth of the pseudo-potential well $\bar{D}_{z,\,\mathrm{injec}}$ in the $z$ direction will be increased by a factor ${Z_0}^2/{R_0}^2$ in the $r$ direction. The depth value is proportional to the $m_a {q_z}^2$ (or $q_z V$) factor which rationalizes the weak trapping efficiencies at low $q_z$ values. Furthermore, for a particular $m_a/z_a$ and a similar low $m/z$ cut-off value (i.e. 50 Th), and keeping the $q_{z,\,\mathrm{injec}}$ value proportional to $q_{z,\,\mathrm{eject}}$, when the $m/z$ range is increased from 2000 Th [i.e. standard (st) mode, $q_{z,\,\mathrm{eject}} = 0.78$] to 3400 Th [i.e. extended (ext) mode, $q_{z,\,\mathrm{eject}} = 0.45$], the $q_{z,\,\mathrm{injec}}$ ratio can be expressed as follows:

$$\frac{[q_{z,\,\mathrm{injec}}]_{\mathrm{st}}}{[q_{z,\,\mathrm{injec}}]_{\mathrm{ext}}} = \frac{[q_{z,\,\mathrm{eject}}]_{\mathrm{st}}}{[q_{z,\,\mathrm{eject}}]_{\mathrm{ext}}} \tag{4}$$

which corresponds to the ratio 0.78/0.48 = 1.73. Hence the $\bar{D}_{z,\,\mathrm{injec}}$ ratio in the two modes is given by

$$\frac{[\bar{D}_{z,\,\mathrm{injec}}]_{\mathrm{st}}}{[\bar{D}_{z,\,\mathrm{injec}}]_{\mathrm{ext}}} = \left(\frac{[q_{z,\,\mathrm{injec}}]_{\mathrm{st}}}{[q_{z,\,\mathrm{injec}}]_{\mathrm{ext}}}\right)^2 \approx 3 \tag{5}$$

Hence it appears that under the extended mode conditions, the number of possible stored ions without space charge is approximately three times lower than that in the standard mode. It follows that this change of mode requires a decrease in the accumulation time to avoid space charge effects. This results from such effects as peak shifting associated at least with (i) resolution loss and (ii) the presence of a long tail toward higher $m/z$ ratios [Fig. 2(c), see below] and also the loss of the weak intensity peaks at lower $m/z$ ratios (e.g. $m/z$ 447 and 451). This is illustrated by changes in the positive ion mass spectrum of substance P when it is recorded in the extended mode instead of the standard mode.

The large space charge effects clearly appear despite a fivefold decrease in accumulation time [i.e. 37 ms, Fig. 2(c)] with respect to 200 ms in the standard mode conditions [Fig. 2(a)]. The 40-fold decrease in accumulation time in the extended mode [i.e. 5 ms, Fig. 2(b)] yields an improved mass spectrum where peaks appear at the expected $m/z$ positions with a sufficient resolution. The positive ion ESI mass spectrum of substance P recorded under these experimental conditions [extended mode with 5 ms accumulation time, Fig. 2(b)] allows us to detect additional peaks at $m/z$ 447, 451, 546 and 548 [Fig. 2(b)]. These new peaks correspond to the $[M + 3H - H_2O/NH_3]^{3+}$, $[M + 3H]^{3+}$, $\mathbf{b}_9^{2+}$ and $\mathbf{y}_9^{2+}$ ions, respectively. The occurrence of these ions at lower $m/z$ ratio during the analytical scan in the extended mode [Fig. 2(b)] is in contrast with that observed in the standard mode [Fig. 2(a)].

This can be explained since the kinetic energy carried by $[M + 2H]^{2+}$ ions is higher in the standard mode than in the extended mode. The kinetic energy $\langle E \rangle_{\mathrm{OSC}}$ value for the ion in the $z$-direction during one secular cycle (OSC) is calculated from the following equation:[32]

$$\langle E \rangle^z_{\mathrm{osc}} = \left| \frac{ze\bar{D}_z}{2} \right| \tag{6}$$

This $\langle E \rangle^z_{\mathrm{OSC}}$ value increases from the extended mode to the standard mode and this increase can be estimated

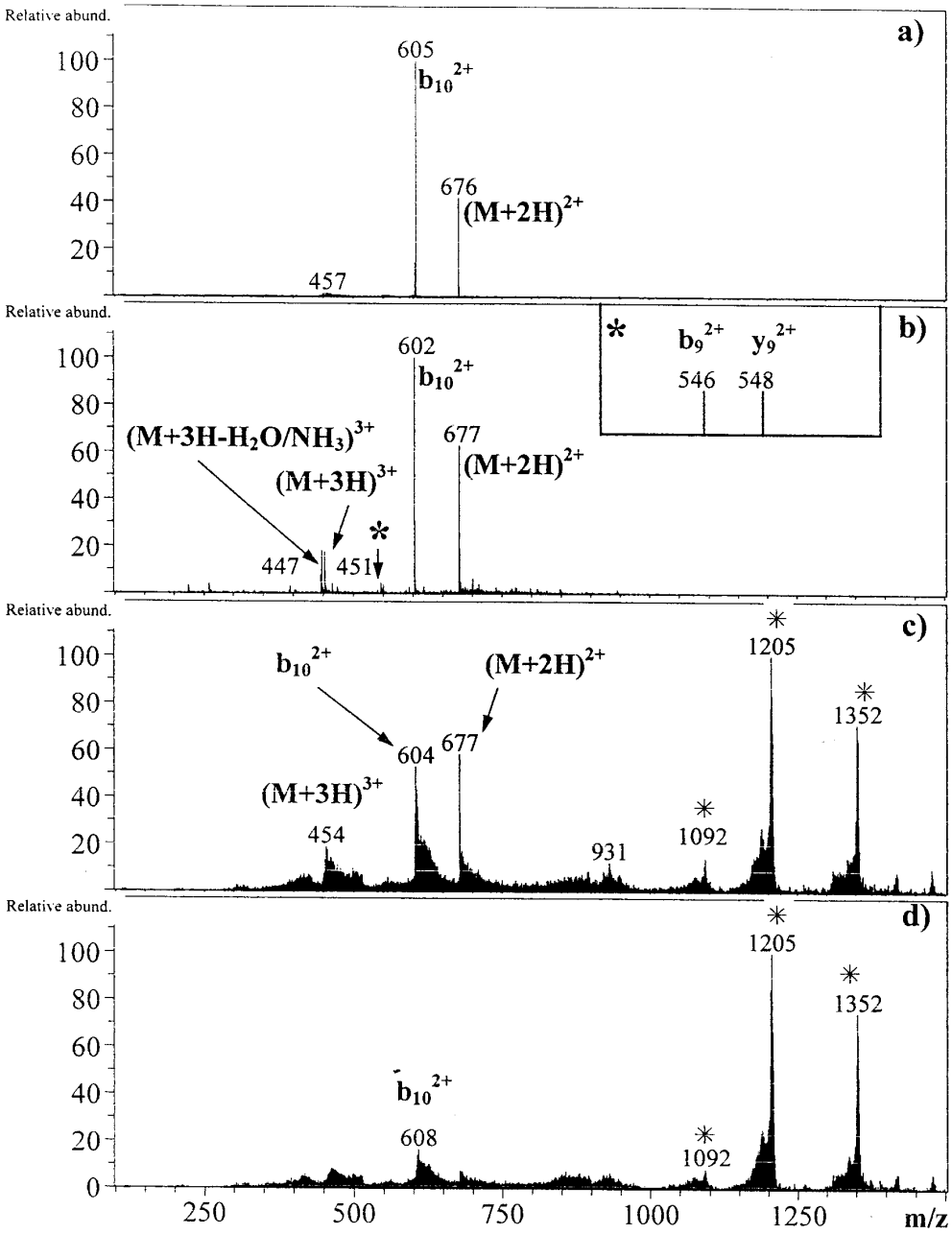


**Figure 2.** ESI mass spectra (average of 10 mass spectra summations) of positive ions of substance P within the 100–1500 Th range, at a capillary exit voltage of 60 V, a skimmer voltage of 10 V, and a low $m/z$ cut-off value of 50 Th, recorded (a) in standard mode ($\beta_{z,\,\mathrm{eject}} = 2/3$) (accumulation time 200 ms) and in extended mode ($\beta_{z,\,\mathrm{eject}} = 1/3$) with the same trapping parameters excepted accumulation times changed to (b) 5, (c) 37 and (d) 49 ms. The ghost peaks are marked with asterisks here and in subsequent figures.

according to Eqns (3a) and (6):

$$\frac{[\langle E\rangle^{z}_{\mathrm{osc}}]_{\mathrm{st}}}{[\langle E\rangle^{z}_{\mathrm{osc}}]_{\mathrm{ext}}} \equiv \left(\frac{0.78}{0.45}\right)^2 \approx 3 \qquad (7)$$

Then, in the standard mode, the $[M + 2H]^{2+}$ ions having higher kinetic energy decompose under collision conditions within higher rate constants and the fragment ions which are not efficiently trapped are not detected as fragment ions (because of a lower $q_z$ value). Furthermore, under space charge conditions, when the $m_b/z_b$ ions are located at $q_z$ values close to that of an abundant $m_a/z_a$ ion, such as $(m_b/z_b) < (m_a/z_a)$, then very broad peaks characterize the $m_b/z_b$ ions. These signals can be lost in the background and transformed into a broad peak with weak intensity. This alternative can also explain absence of ions at the lower $m/z$ values [Fig. 2(a)].

The $m/z$ shift from $m/z$ 602 [Fig. 2(b)] to 605 [Fig. 2(a)] can be rationalized by space charge effects created by the $m/z$ 676 ions [Fig. 2(a)]. Indeed, recent studies[20,31,33] of the space charge influence on peak position on the $m/z$ scale have shown that the stability diagram is moved towards higher $q_z$ values. Consequently, the $q_{z,\,\mathrm{eject}}$ value (i.e. $\beta_z = 1$) is shifted to higher values than the $q_z = 0.908$ limit. This means that the ion secular frequencies are shifted toward lower frequency values and ions are ejected later, i.e at higher r.f. drive voltage values.

The next finding from the mass spectra of substance P recorded in the extended mode concerns the effect of

a long accumulation time {i.e. 37 ms, [Fig. 2(c)]} on the occurrence of artefact peak series, with tails towards lower $m/z$ ratios in the high $m/z$ range, in contrast with that observed with peaks related to the expected ions {i.e. the shifted peaks at $m/z$ 454, 604 and 677 [Fig. 2(c)]}. The former unexpected peaks are located at approximately $m/z$ 1205 and 1352, corresponding to twice the calculated values of $m/z$ 601 and 676 {i.e. the $\mathbf{b}_{10}^{2+}$ and $[M + 2H]^{2+}$ ions, respectively, [Fig. 1(a)]}, in addition to a less abundant ion at $m/z$ 1092, which could correspond to twice the $m/z$ 546 value (i.e. the $\mathbf{b}_{9}^{2+}$ ion). This could be rationalized by assuming that these artefact peaks correspond to singly charged ions such as $\mathbf{b}_{10}^{+}$, $[M + H]^{+}$ and $\mathbf{b}_{9}^{+}$, respectively, which were ejected under particular conditions. Since these artefacts were not observed in the ESI mass spectrum recorded within a shorter accumulation time such as 5 ms [Fig. 2(b)], then they should come from a different origin to the normally ejected ions and correspond neither to protonated molecules (or singly charged fragment ions) nor to alternative doubly charged proton-bound homodimeric species (see below). In fact, they must be considered as ghost peaks, as emphasized previously, because their abundance is reinforced in ESI mass spectra recorded in the extended mode with a longer injection time {e.g. 49 ms, [Fig. 2(d)]}, where the space charge effects are enhanced since the depth of the pseudo-potential well is smaller. Moreover, at a 49 ms accumulation time, the intensities of the $m/z$ 602 and 677 peaks are strongly decreased and these signals are diluted in the background, which is consistent with the existence of intense space charge conditions.

Under negative ion conditions, when the ESI mass spectrum of d(TTGG) is recorded in the extended mode (Fig. 3), the abundance of the singly charged deprotonated molecules is strongly enhanced compared with the triply charged $[M - 3H]^{3-}$ ion (i.e. $m/z$ 404) and the doubly charged $[M - 2H]^{2-}$ ion (i.e. $m/z$ 603) displayed in the ESI mass spectrum recorded in the standard mode [Fig. 1(b)]. This effect cannot result from ion injection because in the extended mode, this step occurs at a lower $q_z$ value (i.e. lower r.f. drive voltage), and then the multiply charged ions should be less excited by collisional activation during the injection step. Alternatively, under extended mode conditions, the ion cloud is subjected to space charge effects and then ion excursions toward the end-caps and/or the circular electrode are associated with an increase in the ion kinetic energy, leading to ion desolvation and collision-induced dissociation (CID). This makes unfavorable the observation of higher multiply charged ions (see above).

Moreover, artefacts are also displayed (Fig. 3). At approximately twice the expected $m/z$ 1207 value (experimental value at $m/z$ 1212, related to the deprotonated $[M - H]^{-}$ molecule), a ghost peak appears at $m/z$ 2516. This signal is broad and hence its position is not accurately determined. However, it could be representative of a possible proton-bound homodimer such as $[M_2 - H]^{-}$, but this will be ruled out later.

### Influence of ion transmission on injection yield and, consequently, on space charge and ghost peak intensities

Ion transmission is significantly enhanced by the increase in the capillary exit voltage in an ESI external source.[34] The amount of ions injected into the ion trap cell leads to a space charge inflation (see below). On the other hand, for a given capillary exit–skimmer potential difference, variation of the capillary exit voltage modifies the relative ion abundances. Consequently, for the substance P sample, a weaker capillary exit potential favors transmission of lower $m/z$ ions, enhancing ion detection as observed in Fig. 4(a) (i.e. capillary exit voltage 30 V) compared with Fig. 2(b) (i.e. capillary exit voltage 60 V) recorded in the extended mode. Hence this explains why the abundances of the multiply charged $[M + 3H - H_2O/NH_3]^{3+}$, $[M + 3H]^{3+}$ and $[M + 2H]^{2+}$ ions ($m/z$ 447 shifted to 448, $m/z$ 451 to 452 and $m/z$ 677 unshifted) are particularly enhanced in Fig. 4(a). Under the last experimental conditions without extended space charge, ions at twice the expected $m/z$ values (i.e. ghost peaks) were not detected.

Conversely, at a higher capillary exit voltage such as 80 V, artefact peaks accompanied by a particular tail structure towards lower $m/z$ values appear at $m/z$ 1092, 1205 and 1353, the last one being the base peak [Fig. 4(b)]. Furthermore, the 'normal' $m/z$ 602 and 677 ions (with tail towards higher $m/z$ values) are less abundant and the $m/z$ 448 and 452 ions disappear in the local noise related to the total loss of resolution. Actually, a new ion appears as an additional unresolved $m/z$ 511 signal which should correspond to twice the $m/z$ 258 ion (a new resolved peak corresponding to the $\mathbf{b}_{2}^{+}$ ion).

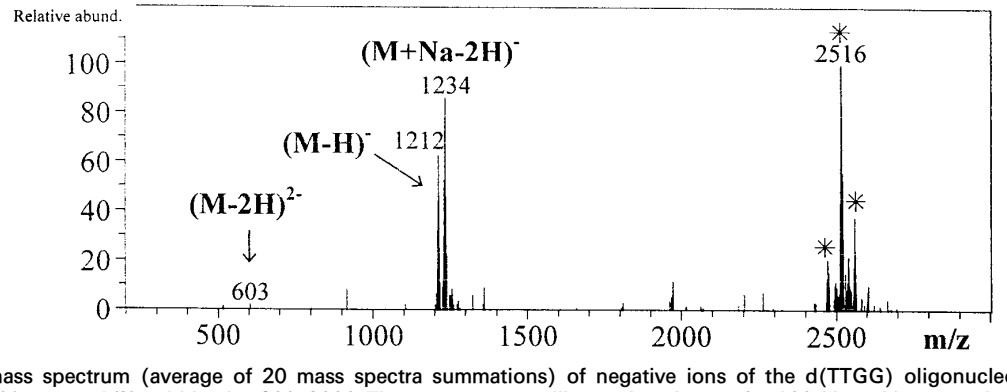


**Figure 3.** ESI mass spectrum (average of 20 mass spectra summations) of negative ions of the d(TTGG) oligonucleotide recorded in extended mode ($\beta_{z,\,\mathrm{eject}} = 1/3$) within the 200–3000 Th range, at a capillary exit voltage of −100 V, a skimmer voltage of −10 V, an accumulation time of 100 ms and a low $m/z$ cut-off value of 100 Th.

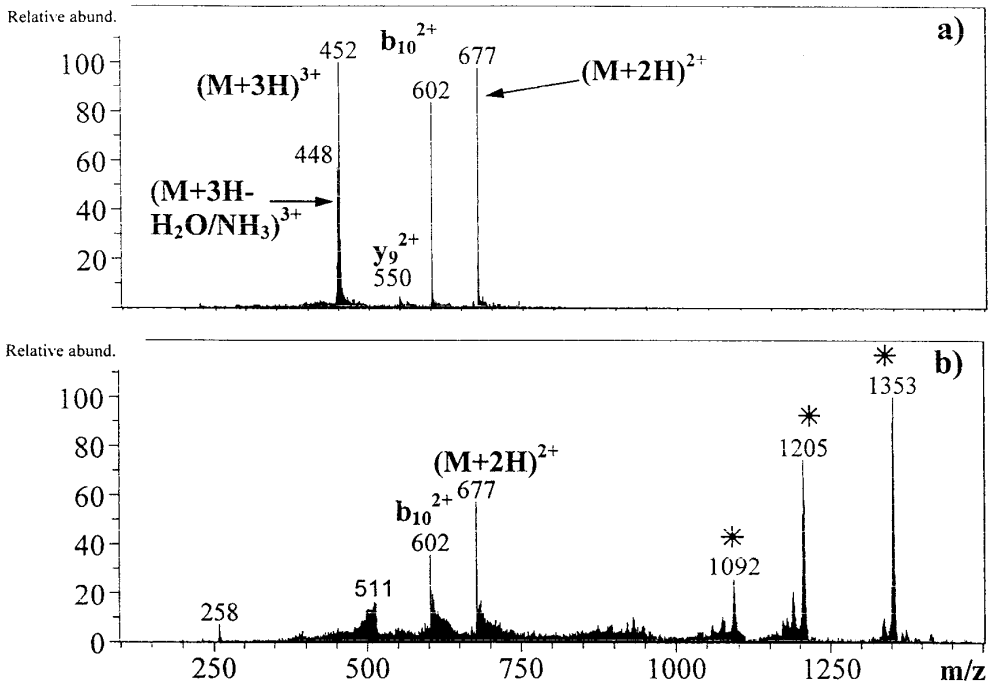


**Figure 4.** ESI mass spectra (average of 10 mass spectra summations) of positive ions of substance P recorded in extended mode ($\beta_{z,\,eject} = 1/3$) within the 100–1500 Th range, at a skimmer voltage of 10 V, an accumulation time of 30 ms and a low *m/z* cut-off value of 50 Th. The capillary exit potentials were (a) 30 and (b) 80 V.

The trend displayed in this ESI mass spectrum is explained by considering that at a higher capillary exit voltage, an improved ion transmission leads to enlargement of the space charge in the ion trap comparable to that reached at higher accumulation times. Note that this ion transmission is associated with the kinetic energy increase of the injected ions related to the difference between the capillary exit and skimmer voltage, which becomes 70 V [Fig. 4(b)] instead of 20 V [Fig. 4(a)]. This is the case for the *m/z* 602 and 677 ions, which at a capillary exit voltage of 80 V efficiently decomposed into the *m/z* 258 (or 452) fragment ion. Alternatively, this effect would imply the disappearance of the *m/z* 1092, 1205 and 1353 ions if these ions were assumed to be proton-bound homodimeric species. The survival of these ion species in spite of the high capillary exit potential used allows one to rule out the existence of such proton-bound dimers.

## Ghost peak properties by using isolation sequence

From the previous experiments, no direct evidence is provided to establish whether these signals considered as ghost peaks correspond to real ions or not. The main finding allowing the observation of these strange-shaped peaks requires the presence of sufficient space charge conditions. In order to obtain more information about these peaks, structural analysis of the corresponding ions would be very useful. For this purpose, under sufficiently large space charge conditions {i.e. leading to a total loss of ions detected at normal *m/z* values, [Fig. 5(a)]} the ions considered as ghost peaks were selected to perform CID experiments. Mass spectra recorded under such experimental conditions, e.g. with 10 ms [Fig. 5(a)] and 100 ms [Fig. 6(a)] accumulation times, display exclusively ghost peaks. Isolation of ions corresponding to such ghost peaks (i.e. *m/z* 1205 and 1352) cannot be achieved because under these ion selection conditions, neither the isolated ion species nor fragment ions at lower *m/z* values, due to spontaneous dissociations, were observed (spectra not reported).

In order to eliminate ambiguity between an inadequate choice of isolation parameters or the presence of spontaneous dissociations, the isolation of particular ions characterized by normal peaks at *m/z* 602 and 677 which were injected without space charge conditions (i.e. 2 ms accumulation time) was successfully performed (data not shown). Nevertheless, suspecting that the ghost peaks originated from the same ions which yield normal signals (even if they are not detected), isolations of the absent ions at *m/z* 602 and 677 were achieved under space charge conditions (i.e. 10 and 100 ms accumulation times reported in Figs 5 and 6, respectively). The mass spectra obtained after the *m/z* 602 and 677 ion isolation by using a 10 ms accumulation time [Figs 5(b) and (c), respectively] display with resolution the selected ions at the normal position, i.e. *m/z* 602 and 677 ions without the presence of ghost peaks, although ghost peaks are exclusively observed in the ESI full mass spectrum [Fig. 5(a)]. This behavior can be rationalized by considering that ion isolation step leads to the ejection of many ions avoiding the space charge effects and, consequently, the detection of ghost peaks.

When the accumulation time is raised to 100 ms, space charge effects increase strongly as expected [Fig. 6(a)] and then, by application of the isolation sequence on the *m/z* 602 [Fig. 6(b)] and *m/z* 677 [Fig. 6(c)] ions, the selected ion spectra display only broad ghost peaks at *m/z* 1205 (and 1069) and *m/z* 1353 (and 1089), respectively. This means that the space charge conditions

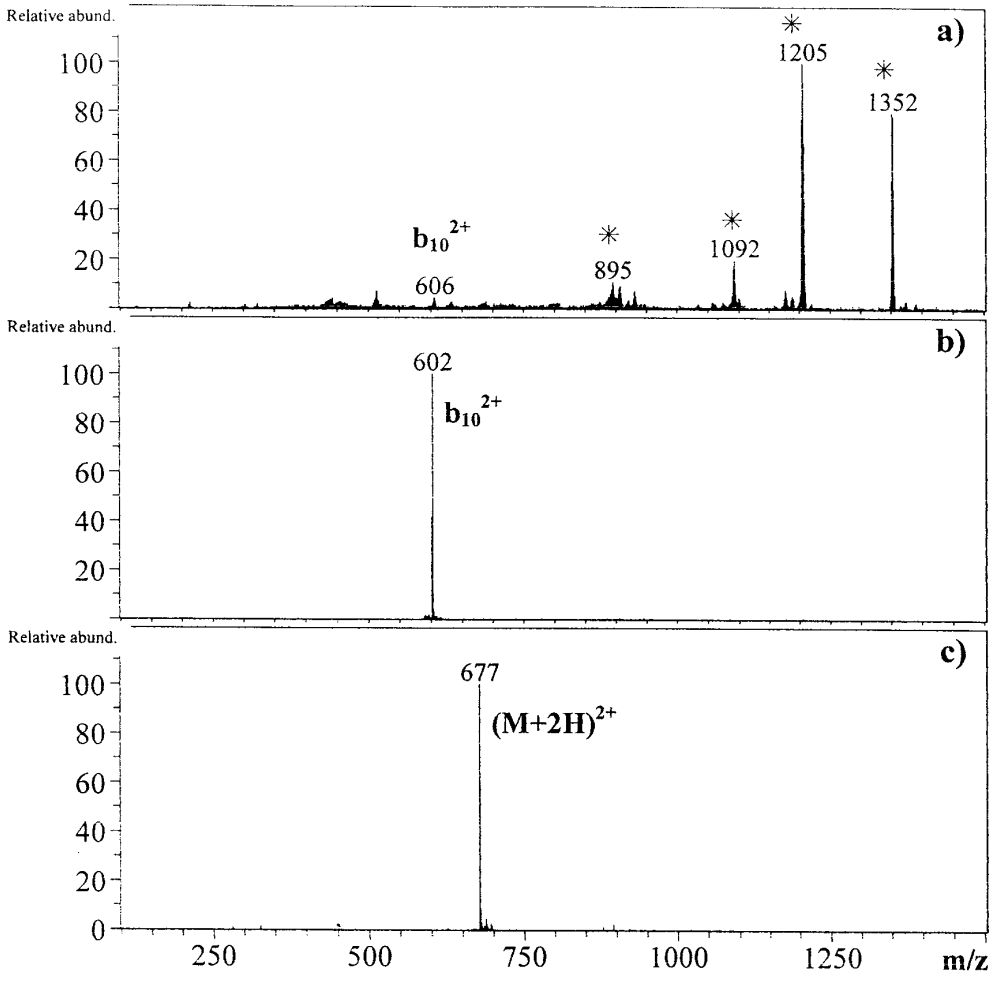


**Figure 5.** ESI mass spectra (average of 10 mass spectra summations) of positive ions of substance P recorded in extended mode ($\beta_{z,\,eject} = 1/3$) within the 100–1500 Th range, at a capillary exit voltage of 60 V, a skimmer voltage of 10 V, an accumulation time of 10 ms and a low $m/z$ cut-off value of 50 Th, recorded (a) without ion selection and with ion selection conditions for (b) $m/z$ 602 and (c) $m/z$ 677.

cannot be avoided to allow the detection of selected ions at the normal position with sufficient resolution.

### Influence of the origin of the mass scan

The role played by the analytical scan is not easy to rationalize, because it modifies strongly the abundance of the ghost peaks. The following experiments were therefore performed to ascertain the real origin of these ghost peaks. The mass spectra of substance P, reported in Fig. 7, were all acquired in the extended mode by using different analytical scan ranges, from various low $m/z$ limits to 1500 Th.

Only the $m/z$ 514, 1092, 1205 and 1352 signals previously considered as ghost peaks are detected within sensitivity when the analytical scan range was 50–1500 Th. Under these conditions, the last ghost peak appears as the base peak in the ESI mass spectrum [Fig. 7(a)]. If the analytical scan is applied from 360 to 1500 Th [Fig. 7(b)], the contribution of ghost peaks decreases in favor of 'normal' peaks (i.e. $m/z$ 603 and mainly $m/z$ 677). Starting the analytical scan from 380 Th instead of 360 Th [Fig. 7(c)] modifies significantly the appearance of the mass spectrum, ghost peaks having nearly disappeared, and this value seems to be a limit for the detection of ghost peaks within large abundances. The mass spectrum recorded from 450 to 1500 Th [Fig. 7(d)] presents quasi-exclusively 'normal' peaks without artefacts (i.e. less than 10% of the base peak at $m/z$ 602). Note that under these conditions, signals of lower $m/z$ values (i.e. $m/z$ 456 and 602) are increased, as the peak resolution, which means that space charge now plays a minor role.

Moreover, this behavior is also observed in the ESI mass spectrum of d(TTGG) obtained in the negative ion extended mode (Fig. 8). In the mass spectrum [Fig. 8(a)], recorded with an analytical scan ranging from 700 to 3000 Th, a ghost peak appears at $m/z$ 2440 (as the base peak) in spite of the weak sensitivity. If the analytical scan range is lowered from 800 to 3000 Th [Fig. 8(b)], the intensity of this ghost peak is significantly decreased compared with that of the 'normal' peak (i.e. $m/z$ 1210). The $m/z$ ratios are shifted because of space charge effects. If the analytical scan range is lowered from 900 to 3000 Th [Fig. 8(c)], the ghost peak disappears, unlike the expected $m/z$ 1207 ion, which is strongly enhanced. A gain in sensitivity and resolution is also observed under the last conditions.

This general behavior seems to be related to the $q_z$ value of the injected ions at the beginning of the analytical scan. Table 1 gives the $q_z$ values of the positive $m/z$

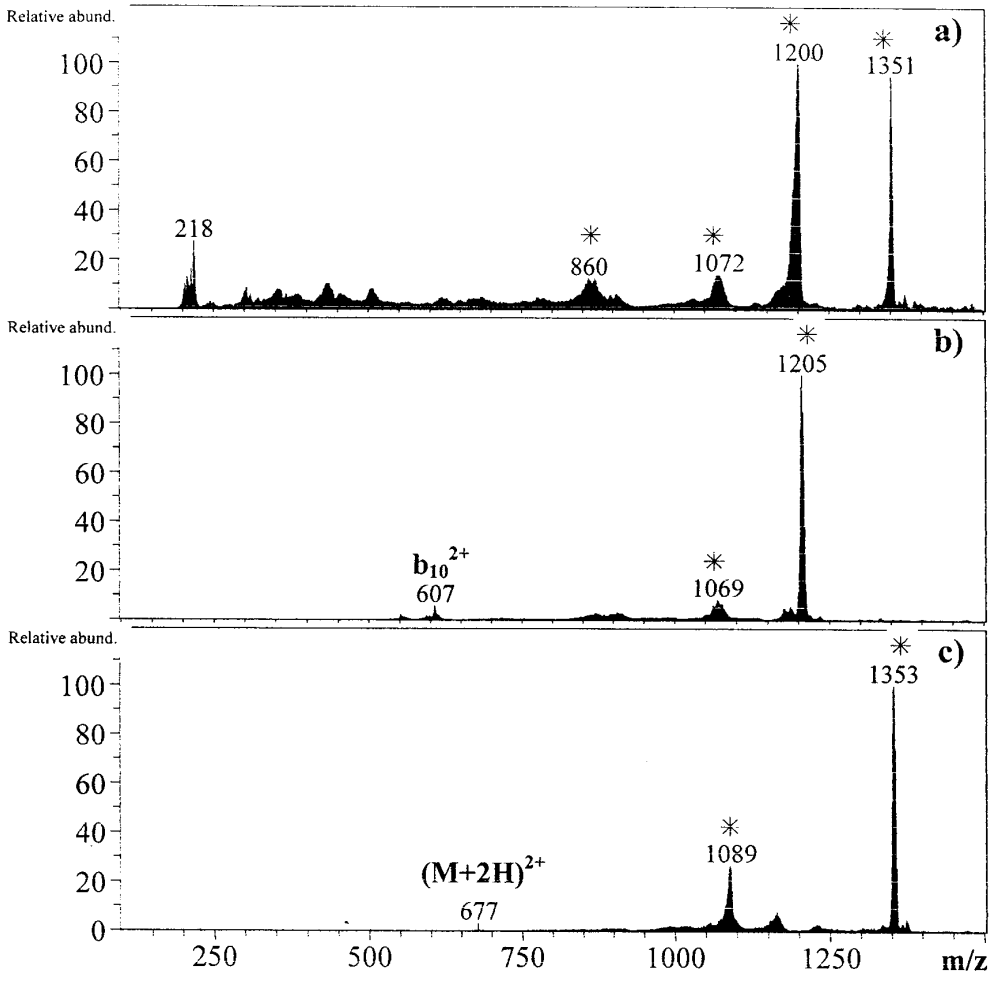


**Figure 6.** ESI mass spectra (average of 10 mass spectra summations) of positive ions of substance P recorded in extended mode ($\beta_{z,\,eject} = 1/3$) within the 100–1500 Th range, at a capillary exit voltage of 60 V, a skimmer voltage of 10 V, an accumulation time of 100 ms and a low *m/z* cut-off value of 50 Th, recorded (a) without ion selection and with ion selection conditions for (b) *m/z* 602 and (c) *m/z* 677.

602 and 677 ions of substance P and of the negative *m/z* 1207 ion of d(TTGG) for the different analytical mass scans described here. Ghost peaks are observed when the analytical scan starts at a $q_z$ value close to or below 0.25 within the error due to the shift of stability diagram, in relation to the space charge effects. This value of 0.25 corresponds to the non-linear resonance at $\beta_z = 2/11$.

Similar behavior characterizes the peaks displayed in the ESI mass spectra of the tripeptide FFF ($M_r = 460$

**Table 1. Theoretical $q_z$ values (calculated without account for space charge effects on the stability diagram shifting) of different ions at the beginning of the analytical scan in *extended* mode**

| | | Ions (*m/z*) and $q_z$ locations | | | |
|---|---|---|---|---|---|
| Substance P | Analytical scan (Th) | *m/z* 601 ($b_{10}^{2+}$) | *m/z* 676 $[M+2H]^{2+}$ | *m/z* 1205 | *m/z* 1353 |
| (Figure 7a) | 50–1500 | 0.038 | 0.033 | 0.019 | 0.017 |
| (Figure 7b) | 360–1500 | 0.269 | 0.239 | 0.134 | 0.120 |
| (Figure 7c) | 380–1500 | 0.284 | 0.253 | 0.142 | 0.126 |
| (Figure 7d) | 450–1500 | 0.336 | 0.299 | 0.168 | 0.150 |
| d(TTGG) | | | | *m/z* 1207 $[M-H]^-$ | *m/z* 2440 |
| (Figure 8a) | 700–3000 | | | 0.261 | 0.130 |
| (Figure 8b) | 800–3000 | | | 0.298 | 0.149 |
| (Figure 8c) | 900–3000 | | | 0.336 | 0.168 |
| FFF peptide | | *m/z* 268 ($a_2^+$) | *m/z* 295 ($b_2^+$) | *m/z* 461 $[M+H]^+$ | *m/z* 921 $[M_2+H]^+$ |
| (Figure 9b) | 250–2000 | 0.420 | 0.380 | 0.242 | 0.122 |
| (Figure 9c) | 300–2000 | | | 0.290 | 0.147 |

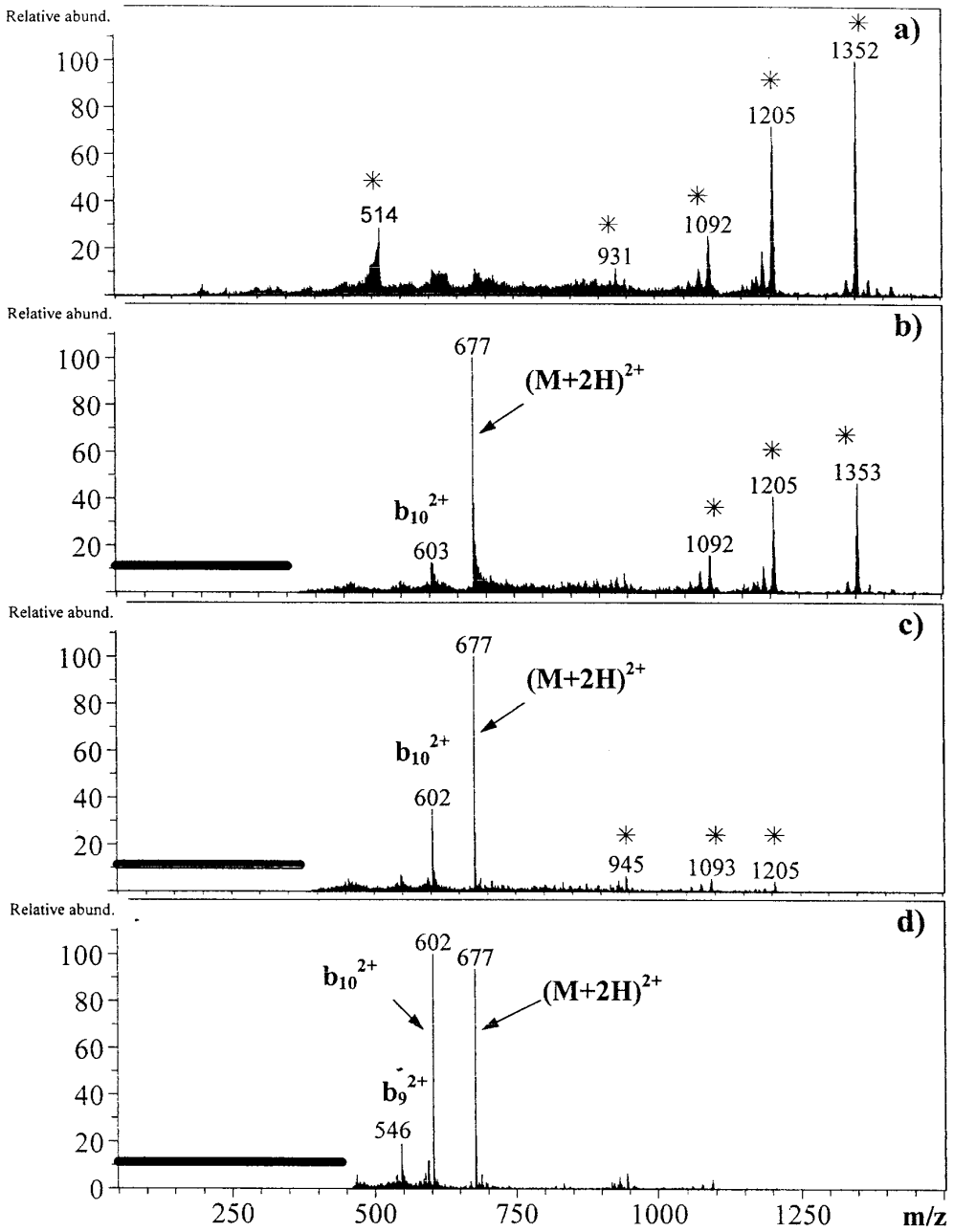


**Figure 7.** ESI mass spectra (average of 10 mass spectra summations) of positive ions of substance P recorded in extended mode ($\beta_{z,\,\mathrm{eject}} = 1/3$) at a capillary exit voltage of 80 V, a skimmer voltage of 10 V, an accumulation time of 100 ms and a low $m/z$ cut-off value of 50 Th, within (a) 50–1500, (b) 360–1500, (c) 380–1500 and (d) 450–1500 Th $m/z$ ranges.

u). Recorded in the standard mode [Fig. 9(a)], the mass spectrum presents, in addition to the $[M + H]^+$ ion at $m/z$ 461, three singly charged fragment ions at $m/z$ 268, 295 and 313, corresponding to the $\mathbf{a}_2{}^+$, $\mathbf{b}_2{}^+$ and $\mathbf{y}_2{}^+$ ions, respectively. Probably a proton-bound homodimer ion $[M_2 + H]^+$ is also observed at $m/z$ 921. The ESI mass spectrum recorded in the extended mode [Fig. 9(b)], with an analytical scan from 250 to 2000 Th, displays four peaks. The base peak at $m/z$ 465 corresponds to the $[M + H]^+$ ion. The shift of the $m/z$ ratio towards higher values is due to the space charge caused by the long ion accumulation time. The second broad but less intense peak at $m/z$ 586 is very likely the ghost peak of the $\mathbf{b}_2{}^+$ ion ($m/z$ 295), which is not detected as a normal peak, in contrast to what is observed in the standard mode. The last ion at $m/z$ 926 could correspond not only to the broad ghost peak of the $[M + H]^+$ ion with a tailing towards lower $m/z$, but also to the proton-bound homodimer $[M_2 + H]^+$ ion, which is observed with very low abundance at $m/z$ 921 in the standard mode. Moreover, a very weak peak at $m/z$ 1840 is detected, which can only correspond to the ghost peak of the proton-bound homodimer $[M_2 + H]^+$ observed in the standard mode. This last assumption agrees with the fact that peaks at $m/z$ 586 and 926 are ghost peaks and not homodimeric ions. If the peak at $m/z$ 1840 corresponds to a tetrameric ion, the mass spectrum would display a peak related to a trimeric ion expected at $m/z$ 1381, which was not detected.

The ghost peaks nearly disappear when the analytical scan applied starts from 300 instead of 250 Th [Fig. 9(c)]. This result suggests that the $q_{z,\,\mathrm{inject}}$ value has a

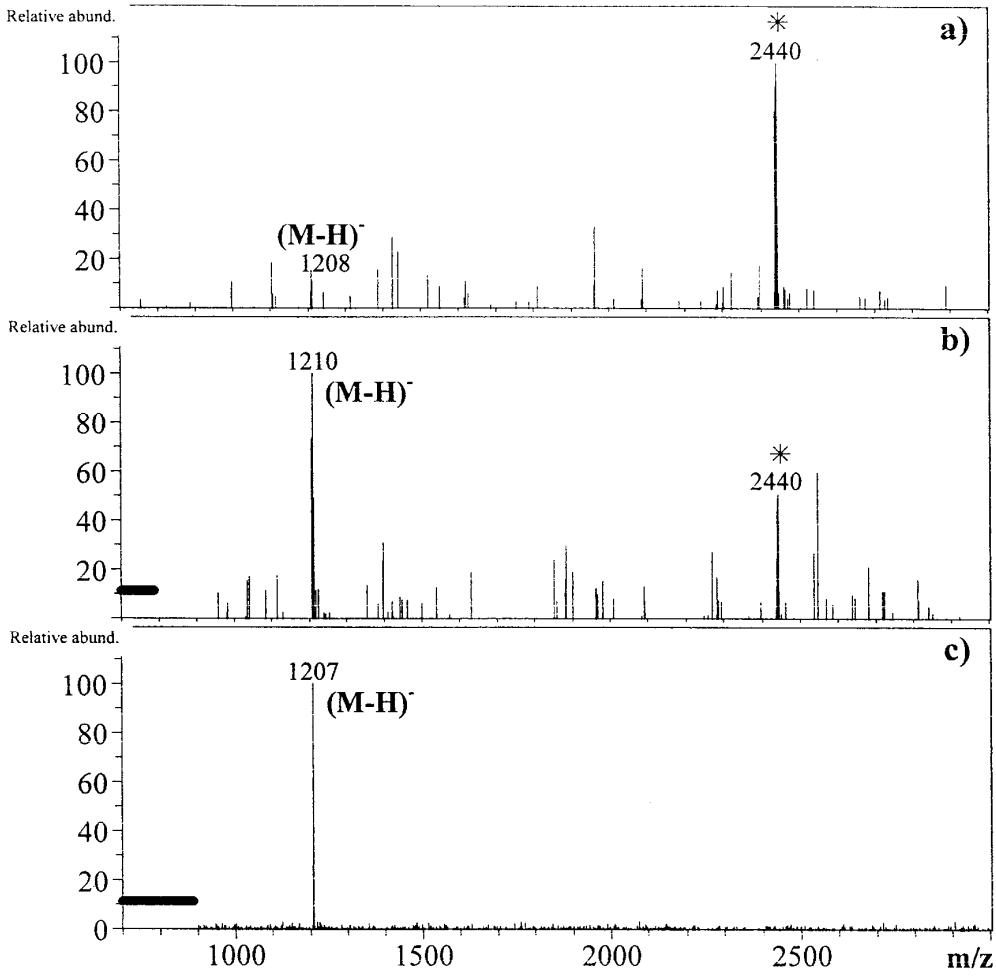


**Figure 8.** ESI mass spectra (average of 50 mass spectra summations) of negative ions of d(TTGG) recorded in extended mode ($\beta_{z,\,eject}$ = 1/3) at a capillary exit voltage of −100 V, a skimmer voltage of −20 V, an accumulation time of 100 ms and a low *m/z* cut-off value of 100 Th, within (a) 700–3000, (b) 800–3000 and (c) 900–3000 Th *m/z* ranges.

profound influence on the detection of ghost peaks. Actually, if the ion is located at a $q_z$ value above 0.25 (approximately calculated without space charge, Table 1) at the origin of the analytical scan, it cannot appear as a ghost peak in the mass spectrum, whereas if this $q_z$ value is below 0.25, ion signals are observed as ghost peaks. This particular $q_z$ value, as emphasized previously, corresponds to the non-linear resonance at $\beta_z = 2/11$, which is related to the ejection value for the high mass range.

Thus, when the analytical scan starts from 250 Th [Fig. 9(b)], the $[M + H]^+$ ion is shifted to *m/z* 465 and its $q_z$ value of 0.242 is close to $q_z = 0.25$, the value required for the observation of a ghost peak at twice the *m/z* ratio, i.e. *m/z* 926. However, the ghost peak at *m/z* 586 should not be observed for the corresponding $\mathbf{b}_2^+$ fragment ion, expected at *m/z* 295. Indeed, the $q_z$ position of this ion is located at $q_z = 0.38$ (Table 1) at the analytical scan start, a value significantly higher than the 0.25 limit. Nevertheless, it appears as a broad, unexpected peak at *m/z* 586 without detection of the normal *m/z* 295 signal.

This result can be rationalized by considering that during the analytical scan, a spontaneous fragmentation of the $[M + H]^+$ ion (*m/z* 465) into a $\mathbf{b}_2^+$ ion (*m/z* 295) takes place at least partially. However, under the analytical scan conditions, during the metastable decompositions, the $\mathbf{b}_2^+$ ion produced must be located, *a priori*, at $q_z \geq 0.38$ (close to $q_{z,\,eject} = 0.45$), which does not allow the detection of $\mathbf{b}_2^+$ as a ghost peak, which is inconsistent with the experimental results. In order to explain these results, additional assumptions will be required based upon the fact that the $[M + H]^+$ ion can yield both the normal *m/z* 465 peak and ghost *m/z* 926 signal depending on the importance of the space charge. The $[M + H]^+$ ion characterized as a normal peak can spontaneously decompose in addition to that related to the ghost peak. After metastable decomposition, the former yields the $\mathbf{b}_2^+$ ion at *m/z* 295 (not observed) and the latter leads to the $\mathbf{b}_2^+$ ion at *m/z* 586 as a ghost peak. These assumptions will be supported by further experiments which are in progress.

However, when the analytical scan begins at 300 instead of 250 Th [Fig. 9(c)], the $[M + H]^+$ ion (*m/z* 465) is characterized by $q_z = 0.290$, i.e. above 0.25, so it cannot give rise to a ghost peak, which is consistent with our assumptions. That is why the *m/z* 586 and 926 ghost peaks have nearly disappeared. This is evidence of the role played by the $[M + H]^+$ ion in $\mathbf{b}_2^+$ ion formation as a ghost peak. It can be observed that under space charge conditions, the $q_z$ position of the non-linear resonance at $\beta_z = 2/11$ is shifted to a higher value

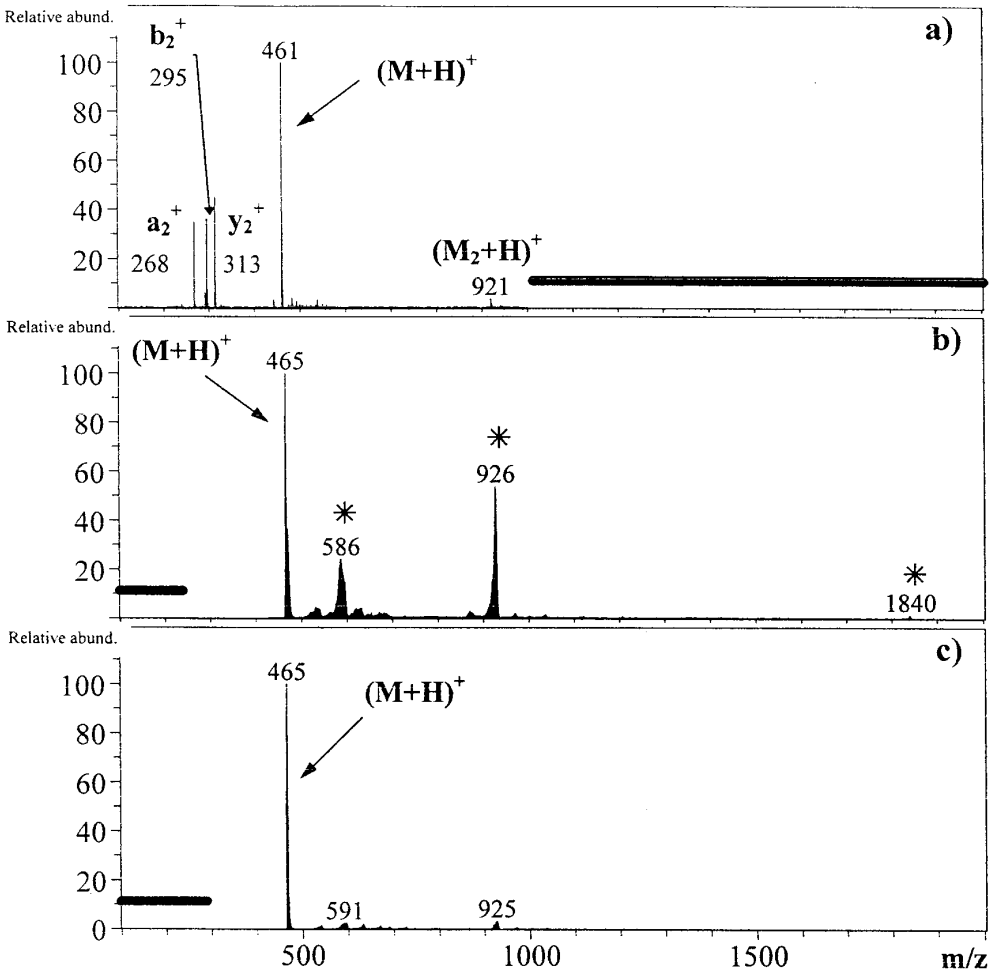


**Figure 9.** ESI mass spectra (average of 10 mass spectra summations) of positive ions of FFF peptide with a low *m/z* cut-off of 50 Th recorded (a) in standard mode ($\beta_{z,\,eject} = 2/3$) within the 100–1000 Th range, at a capillary exit voltage of 80 V, a skimmer voltage of 15 V and an accumulation time of 20 ms and in extended mode ($\beta_{z,\,eject} = 1/3$), at a capillary exit voltage of 60 V, a skimmer voltage of 10 V and an accumulation time of 50 ms, within (b) 250–2000 and (c) 300–2000 Th *m/z* ranges.

and its form is broadened.[28] The observed shift ($\delta q_z$) is positive and varies linearly with the ion abundance.[35] This could explain why for some ions, ghost peaks can appear [e.g. Fig. 8(a)] when the $q_z$ value of the original peak is just higher than 0.25 (Table 1).

## Interpretation of ghost peak appearance

Space charge conditions are the starting point to explain the appearance of ghost peaks. Its observation implies that part of the ions are not at the center of the ion trap, allowing an increase in the amplitude of ion motion, in order to minimize repulsive coulombic forces.[36] The model rationalizes the long tail toward the high *m/z* ratio range accompanying the 'normal' peaks. A spatial distribution of ions from the ion trap center to the end-caps and ring electrodes is assumed. Some ions are close to the center (i.e. $r \approx 0$ and $z \approx 0$), where the amplitude of ion motion increases less than elsewhere, and as the ion amplitude rises by action of space charge, the relative secular frequency drift toward lower values takes place, giving peaks at higher *m/z* values.[37]

The contribution of higher order multipole fields is increased when the ions move away from the ion trap center. Furthermore, it must be considered that for an odd-multipole field, the ion relative secular frequency decreases when its amplitude increases. In the same way, for an even-non-linear positive field, as the ion amplitude enlarges, the secular frequency increases and for an even-negative multipole field as the ion amplitude enlarges, the secular frequency decreases.[38]

During the analytical scan, a set of ions characterized by the same *m/z* ratio first pass through the odd non-linear resonance at $\beta_z = 2/11$ ($q_z = 0.25$). As their kinetic energy rises from this non-linear resonance, their amplitude increases and their relative secular frequency decreases. Under such particular space charge conditions, a complex distribution of motions must characterize the same *m/z* ions. It may be assumed that their distribution results from motions of two varieties of chosen ions distinguished by: (i) small increased amplitudes for ions considered as 'focused ions' and (ii) high increased amplitudes for ions called a 'non-focused ions'. Consequently, these ions must be mainly characterized by two types of frequencies relative to that expected from calculation.

Above $q_z = 0.25$, the 'focused ions' with the lowest amplitudes have the highest relative frequencies, and the 'non-focused ions' have the highest amplitudes and the lowest relative frequencies. In all cases, the relative fre-

quencies are lower than the initial frequency of the considered ions, which is reached just before the ions being submitted to the non-linear perturbation. Close to $\beta_z = 1/3$ (i.e. $q_z = 0.45$), the 'focused ions' which have the highest relative frequencies (and lowest amplitudes) are changed into an ion population with the smallest relative frequencies conserving the lowest amplitudes, and the 'non-focused ions' become the population having (i) the highest relative frequencies (above the relative initial frequency related to the $\beta_z$ values characterizing the considered ions) and also (ii) the highest amplitudes (i.e. $q_z = 0.45$ corresponds to an even-positive multipole field, the relative frequencies increase all the more as the amplitude is raised). On the other hand, this leads to a population frequency reversal, meaning that 'focused ions' with the highest frequencies below $q_z = 0.45$ become, above $q_z = 0.45$, ions with the lowest frequencies. As this occurs near $q_z^{\text{theoretical}} = 0.45$, the 'non-focused ions' are not ejected at this value, in spite of application of the axial modulation for efficient ejection, because their own frequencies are too high, but at $q_z^{\text{real}} = 0.908$ (i.e. the natural boundary $\beta_z = 1$), giving unresolved ghost peaks at twice the expected $m/z$ value $[(m/z)_{\text{real}}]$. The population frequency reversal can explain the low $m/z$ tailing of ghost peaks. This assumption agrees with both the forms (low $m/z$ tail for ghost peaks instead of high $m/z$ tail for 'normal' peaks) and the position of the ghost peaks $[(m/z)_{\text{ghost}}]$ in the mass spectrum. The $m/z$ ratio can be expressed as follows:

$$\frac{(m/z)_{\text{ghost}}}{(m/z)_{\text{real}}} = \frac{q_{z,\,\text{eject}}^{\text{real}}}{q_{z,\,\text{eject}}^{\text{theoretical}}} \tag{8}$$

which corresponds to the ratio $0.908/0.45 = 2$. This explanation implies why ions related to ghost peaks must be located at a $q_z$ value $\leqslant 0.25$ (see above) (this $q_z$ value corresponding to the non-linear resonance at $\beta_z = 2/11$, at the beginning of the analytical scan).

Moreover, under our experimental conditions, the fact that ghost peaks do not appear in the standard mode but do in the extended mode can be interpreted by considering the analytical scan rate. In the standard mode, a full scan from 50 to 2000 Th takes 0.975 s to perform (i.e. a scanning rate of 2000 Th $s^{-1}$), whereas in the extended mode, a full scan from 50 to 3400 Th requires 1.97 s (i.e. a scanning rate of 1700 Th $s^{-1}$). On the other hand, the times for scanning one $q_z$ unit are close to 1.25 and 4.38 s in the standard and extended modes, respectively. The change in the $m/z$ scale used yields a rate decrease of 3.5-fold by enlargement of the mass scale range. Consequently, ions located at a $q_z$ value $<0.25$ (just before starting the analytical scan) move more slowly to $q_z = 0.25$ in the extended mode, according to a lower scan rate, than in the standard mode. During the analytical scan under standard mode conditions, the ions stay at the $q_z = 0.25$ position for a shorter period than in the extended mode. Hence, ions are subjected to the effect of the non-linear resonance at $\beta_z = 2/11$ for a longer time. This effect is especially important when ions are away from the ion trap center (i.e case of the 'non-focused ions'), hindering ion ejection at the normal $\beta_z$ value (i.e. $\beta_z = 1/3$) and enhancing ion ejection at the $\beta_z = 1$ boundary, leading to the observation of ghost peaks.

## CONCLUSION

Among the various investigations on ion–ion interactions resulting in space charge effects, only a few papers have described the occurrence of artefact signals called here 'ghost peaks' in mass spectra recorded by using ion trap mass spectrometer. Such phenomena occur when space charge leads to ion excursion towards the end-caps, where the contribution of the non-linear fields is increased. In a conventional ion trap, these signals appear as broad peaks at $m_{\text{apparent}} = m_{\text{real}}(q_z^{\text{apparent}}/0.908)$, with $q_z^{\text{apparent}} < 0.908$, which means that ion ejection occurs at a $\beta_z$ value $<1$ and that the corresponding peaks appear at lower $m/z$ values than those expected.

In the present study, by using a modified ion trap combined with an external electrospray ion source, which allows ion ejection at lower $q_z$ values than $q_z = 0.908$ (for enlarging the $m/z$ ratio range), ghost peaks were detected at higher $m/z$ values than those expected for normal ions. They appear when the ion ejection during the analytical scan takes place at $\beta_z = 1/3$ (i.e. $q_z = 0.45$) instead of $\beta_z = 2/3$ or 1. These signals are characterized by $m/z$ values at twice the expected values and this requires space charge conditions, so automatic gain control was not used. The positions of these artefacts are unaffected by these space charge effects and in contrast with the normal signals which are shifted toward higher $m/z$ values. However, the shape of ghost peaks is broader and the tail is spread out towards lower $m/z$ values in comparison with normal peaks shifted to higher $m/z$ values. Note that both the negative and positive ions are submitted to the same behavior. Examination of the intensity of such signals shows that they are exclusively dependent upon the space charge produced during the ion injection step (i.e. by the improvement of the ion transmission and by the increase in the ion accumulation time). Nevertheless, their efficient observation requires that the $q_z$ position of the analyte ions just prior to applying the analytical scan must be at values lower than 0.25, which corresponds to a non-linear resonance (i.e. $\beta_z = 1/3$). Under such conditions, the ion cloud motion is strongly affected and then the ion ejection occurs inefficiently at higher r.f. drive potential amplitudes related to the $q_z = 0.45$ value. Consequently, a large fraction of analyte ions were not ejected at $\beta_z = 1/3$ and were preserved, before being ejected by the increase in the r.f. drive potential at the natural $\beta_z = 1$ boundary ($q_z = 0.908$). Similar phenomena are very likely to be expected by using a larger mass scale (i.e. ejection at $\beta_z = 2/11$, $q_z = 0.25$) if the space charge is not controlled. The presence of ghost peaks could yield confusion and some misassignments, since formally they correspond to either hydrogen-bonded dimeric ion species or to twice less charged ion species as they could be produced under ESI conditions. However, various tools can be used for distinguishing normal from ghost peaks. In particular, the narrow frequency used as axial modulation could be changed to broadband frequencies for ejecting ions from this particular $q_z$ value (related to the $m/z$ range) to $q_z = 0.908$. A simpler method was applied in this work and concerns the use of the ion isolation at the

apparent $m/z$ value (observation of normal signal even if it was not observed in the ESI mass spectrum).

Rationalization of such phenomena is in progress with experiments in the high range mode (ejection at $q_{z,\,\mathrm{eject}} = 0.25$, $\beta_z = 2/11$). This should help us to understand new properties of non-linear resonances under space charge conditions which defocus the ion cloud from the ion trap center where normally the quadrupolar field contributes to stability of the ion motion in the ion trap.

## Acknowledgement

The authors thank the Centre d'Etudes du Bouchet, Université Pierre et Marie Curie and CNRS for financial support. The technical support of Bruker is gratefully acknowledged.

## REFERENCES

1. (a) R. W. Vachet and G. L. Glish, *J. Am. Soc. Mass Spectrom.* **7**, 1194 (1996); (b) S. A. McLuckey, G. J. Van Berkel, D. E. Goeringer and G. L. Glish, *Anal. Chem.* **66**, 689A (1994); (c) S. A. McLuckey, G. J. Van Berkel, D. E. Goeringer and G. L. Glish, *Anal. Chem.* **66**, 737A (1994); (d) I. A. Kaltashov, V. M. Doroshenko and R. J. Cotter, *Proteins: Struct. Funct. Genet.* **28**, 53 (1997).
2. (a) H. E. Witkowska, B. N. Green, M. Morris and C. H. L. Shackleton, *J. Mass Spectrom.* and *Rapid Commun. Mass Spectrom.* S111 (1995); (b) J. L. Stephenson and S. A. McLuckey, *J. Am. Chem. Soc.* **118**, 7390 (1996).
3. (a) S. A. McLuckey and S. Habibi-Goudarzi, *J. Am. Chem. Soc.* **115**, 12085 (1993); (b) S. A. McLuckey and S. Habibi-Goudarzi, *J. Am. Soc. Mass Spectrom.* **5**, 740 (1994); (c) M. J. Doktycz, S. Habibi-Goudarzi and S. A. McLuckey, *Anal. Chem.* **66**, 3416 (1994); (d) S. A. McLuckey and G. Vaidyanathan, *Int. J. Mass Spectrom. Ion Processes* **162**, 1 (1997).
4. (a) G. J. Van Berkel, G. L. Glish and S. A. McLuckey, *Anal. Chem.* **62**, 1284 (1990); (b) R. Korner, M. Wilm, K. Morand, M. Schubert and M. Mann, *J. Am. Soc. Mass Spectrom.* **7**, 150 (1996); (c) M. E. Bier and J. C. Schwartz, in *Electrospray Ionization Mass Spectrometry*, edited by R. B. Cole, p. 235. Wiley, New York (1997).
5. (a) M. Karas and F. Hillenkamp, *Anal. Chem.* **60**, 2299 (1988); (b) R. C. Beavis and B. T. Chait, *Methods Enzymol.* **270**, 519 (1996); (c) J. C. Schwartz and M. E. Bier, *Rapid Commun. Mass Spectrom.* **7**, 27 (1993); (d) D. H. Russel and R. D. Edmundson, *J. Mass Spectrom.* **32**, 263 (1997); (e) K. Jonscher, G. Currie, A. L. McCormack and J. R. Yates, *Rapid Commun. Mass Spectrom.* **7**, 20 (1993); (f) V. M. Doroshenko and R. J. Cotter, *Rapid Commun. Mass Spectrom.* **7**, 822 (1993).
6. S. F. Wong, C. K. Meng and J. B. Fenn, *J. Phys. Chem.* **92**, 546 (1988).
7. (a) R. E. Kaiser, R. G. Cooks, G. C. Stafford, J. E. P. Syka and P. H. Hemberger, *Int. J. Mass Spectrom. Ion Processes* **106**, 79 (1991); (b) R. E. Kaiser, R. G. Cooks, J. Moss and P. H. Hemberger, *Rapid Commun. Mass Spectrom.* **3**, 50 (1989); (c) R. E. Kaiser, J. W. Louis, J. W. Amy and R. G. Cooks, *Rapid Commun. Mass Spectrom.* **3**, 225 (1989); (d) K. Morand, M. Schubert, J. Franzen and M. Mann, in *Proceedings of the 41st ASMS Conference on Mass Spectrometry and Allied Topics*, San Francisco CA, 1993, p. 706; (e) J. V. Johnson, M. M. Booth, J. L. Stephenson, R. R. Vargas and R. A. Yost, in *Proceedings of the 41st ASMS Conference on Mass Spectrometry and Allied Topics*, San Francisco CA, 1993, p. 712.
8. (a) R. E. Kaiser, R. G. Cooks, G. C. Stafford, J. E. P. Syka and P. H. Hemberger, *Int. J. Mass Spectrom. Ion Processes* **106**, 79 (1991); (b) J. C. Schwartz, M. E. Bier, D. M. Taylor, J. Zhou, J. E. P. Syka, M. S. James and G. C. Stafford, in *Proceedings of the 43rd ASMS Conference on Mass Spectrometry and Allied Topics*, Atlanta GA, 1995, p. 1114.
9. J. F. J. Todd, A. D. Pennan and R. D. Smith, *Int. J. Mass Spectrom. Ion Processes* **106**, 117 (1991).
10. (a) M. Weber-Grabau, P. E. Kelley, S. C. Bradshaw and D. J. Hoekman, in *Proceedings of the 36th ASMS Conference on Mass Spectrometry and Allied Topics*, San Francisco CA, 1988, p. 1106; (b) J. C. Schwartz, J. E. P. Syka and I. Jardine, *J. Am. Soc. Mass Spectrom.* **2**, 198 (1991); (c) J. D. Williams, K. A. Cox, R. G. Cooks, R. E. Kaiser and J. C. Schwartz, *Rapid Commun. Mass Spectrom.* **5**, 327 (1991); (d) J. D. Williams and R. G. Cooks, *Rapid Commun. Mass Spectrom.* **6**, 524 (1992); (e) J. A. Schwartz and I. Jardine, *Rapid Commun. Mass Spectrom.* **6**, 313 (1992); (f) F. A. Londry, G. J. Wells and R. E. March, *Rapid Commun. Mass Spectrom.* **7**, 43 (1993); (g) F. A. Londry and R. E. March, *Int. J. Mass Spectrom. Ion Processes* **144**, 87 (1995).
11. Y. Wang, M. Schubert and J. Franzen, in *Proceedings of the 44th ASMS Conference on Mass Spectrometry and Allied Topics*, Portland OR, 1996, p. 131.
12. (a) F. Guidugli and P. Traldi, *Rapid Commun. Mass Spectrom.* **5**, 343 (1991); (b) R. Alheit, S. Kleineidam, F. Vedel, M. Vedel and G. Werth, *Int. J. Mass Spectrom. Ion Processes* **154**, 155 (1996).
13. F. Guidugli, P. Traldi, A. M. Franklin, M. L. Langford, J. Murell and J. F. J. Todd, *Rapid Commun. Mass Spectrom.* **6**, 229 (1992).
14. M. M. Mann, C. K. Meng and J. B. Fenn, *Anal. Chem.* **61**, 1702 (1989).
15. (a) R. D. Smith, J. A. Loo, C. J. Barinaga, C. G. Edmonds and H. R. Udseth, *J. Am. Soc. Mass Spectrom.* **1**, 53 (1990); (b) R. D. Voyksner and T. Pack, *Rapid Commun. Mass Spectrom.* **5**, 263 (1991); (c) V. Katta, S. K. Chowdhury and B. T. Chait, *Anal. Chem.* **63**, 174 (1991); (d) D. S. Ashton, C. R. Beddell, D. J. Cooper, B. N. Green and R. W. A. Oliver, *Org. Mass Spectrom.* **28**, 721 (1993); (e) A. K. Harrata, L. N. Domelsmith and R. B. Cole, *Biol. Mass Spectrom.* **22**, 59 (1993); (f) O. Laprévote, P. Ducrot, C. Thal, L. Serani and B. C. Das, *J. Mass Spectrom.* **31**, 1149 (1996); (g) I. Mazsaroff, W. Yu, B. D. Kelley and J. E. Vath, *Anal. Chem.* **69**, 2517 (1997); (h) L. Debrauwer, D. Zalko, G. Bories and J. Tulliez, *Rapid Commun. Mass Spectrom.* **11**, 1089 (1997).
16. (a) S. A. McLuckey, D. E. Goeringer and G. L. Glish, *Anal. Chem.* **64**, 1455 (1992); (b) J. C. Schwartz and I. Jardine, *Rapid Commun. Mass Spectrom.* **6**, 313 (1992); (c) V. M. Doroshenko and R. J. Cotter, *Rapid Commun. Mass Spectrom.* **8**, 766 (1994).
17. (a) M. Wang and G. Wells, *ICR*/Ion Trap Newsl. **31**, 29 (1993); (b) Y. Wang, *Rapid Commun. Mass Spectrom.* **7**, 920 (1993); (c) M. Wang and G. Wells, in *Proceedings of the 41st ASMS Conference on Mass Spectrometry and Allied Topics*, San Francisco CA, 1993, p. 463; (d) J. Qin and B. T. Chait, in *Proceedings of the 43rd ASMS Conference on Mass Spectrometry and Allied Topics*, Atlanta GA, 1995, p. 1100.
18. S. A. McLuckey, G. L. Glish and G. J. Van Berkel, *Int. J. Mass Spectrom. Ion Processes* **106**, 213 (1991).
19. S. Grégoire, J. C. Mathurin, R. E. March and J. C. Tabet, *ICR*/Ion Trap Newsl. **43**, 12 (1996).
20. J. C. Mathurin, S. Grégoire, A. Brunot, J.-C. Tabet, R. E. March, S. Catinella and P. Traldi, *J. Mass Spectrom.* **32**, 829 (1997).
21. D. M. Eades, J. V. Johnson and R. A. Yost, *J. Am. Soc. Mass Spectrom.* **4**, 917 (1993).
22. (a) P. Traldi, D. Favretto, S. Catinella and O. Bertolini, *Org. Mass Spectrom.* **28**, 745 (1993); (b) F. A. Londry, R. J. S. Morrison and R. E. March, in *Proceedings of the 43rd ASMS Conference on Mass Spectrometry and Allied Topics*, Atlanta GA, 1995, p. 1124; (c) K. A. Cox, C. D. Cleven and R. G. Cooks, *Int. J. Mass Spectrom. Ion Processes* **144**, 47 (1995);

(d) C. D. Cleven, K. A. Cox, R. G. Cooks and M. E. Bier, *Rapid Commun. Mass Spectrom.* **8**, 451 (1994); (e) W. Mo and J. F. J. Todd, *Rapid Commun. Mass Spectrom.* **10**, 424 (1996); (f) O. Bortoloni and P. Traldi, *Rapid Commun. Mass Spectrom.* **9**, 1470 (1995).
23. B. A. Shaffer, J. Karnicky and S. E. Buttrill, in *Proceedings of the 43rd ASMS Conference on Mass Spectrometry and Allied Topics*, Atlanta GA, 1995, p. 1112.
24. W. Mo, M. L. Langford and J. F. J. Todd, *Rapid Commun. Mass Spectrom.* **9**, 107 (1995).
25. (a) J. Louris, J. C. Schwartz, G. J. Stafford, J. E. P. Syka and D. M. Taylor, in *Proceedings of the 40th ASMS Conference on Mass Spectrometry and Allied Topics*, Washington DC, 1992, p. 1003; (b) S. A. Lammert and J. M. Wells, *Rapid Commun. Mass Spectrom.* **10**, 361 (1996).
26. G. Zon and W. J. Stec, *Oligonucleotides and Analogs: a Practical Approach*. Oxford University Press, New York (1991).
27. R. G. Cooks and A. L. Rockwood, *Rapid Commun. Mass Spectrom.* **5**, 53 (1991).
28. G. C. Stafford, D. M. Taylor, S. C. Bradshaw, J. E. P. Syka and M. Uhrich, in *Proceedings of the 35th ASMS Conference on Mass Spectrometry and Allied Topics*, Denver CO, 1987, p. 775.
29. R. Roepstorff and J. Fohlman, *Biomed. Mass Spectrom.* **11**, 601 (1984).
30. X. J. Tang, P. Thibault and R. K. Boyd, *Anal. Chem.* **65**, 2824 (1993).
31. H. G. Dehmelt, *Adv. At. Mol. Phys.* **3**, 53 (1967).
32. R. E. March and F. A. Londry, in *Practical Aspects of Ion Trap Mass Spectrometry*, edited by R. E. March and J. F. J. Todd, p. 25. CRC Press, Boca Raton, FL (1995).
33. R. Alheit, S. Kleineidam, F. Vedel, M. Vedel and G. Werth, *Int. J. Mass Spectrom. Ion Processes* **154**, 155 (1996).
34. (a) B. Lin and J. J. Sunner, *J. Am. Soc. Mass Spectrom.* **5**, 873 (1994); (b) R. Guevremont, K. W. M. Siu, J. Wang and J. C. Y. Leblanc, in *Proceedings of the 42nd ASMS Conference on Mass Spectrometry and Allied Topics*, Chicago IL, 1994, p. 999.
35. R. Alheit, T. Gudjons, S. Kleineidam and G. Werth, *Rapid Commun. Mass Spectrom.* **10**, 583 (1996).
36. J. H. Parks and A. Szöke, *J. Chem. Phys.* **103**, 1422 (1995).
37. F. Vedel and J. André, *Int. J. Mass Spectrom. Ion Processes* **65**, 1 (1985).
38. (a) J. Franzen, *Int. J. Mass Spectrom. Ion Processes* **125**, 165 (1993); (b) J. Franzen, *Int. J. Mass Spectrom. Ion Processes* **130**, 15 (1994).